Journal of Materials Chemistry B

PAPER

View Article Online
View Journal



Cite this: DOI: 10.1039/d5tb01059d

# Impairing antioxidant protection by diminishing hyaluronic acid using nanoliposomes for tumor therapy†

Hegang Lu,[a] Yunjian Yu,[a] Shengke Zhao,[a] Youtao Xin,[a] Hongyu Liu,[a] Qinghua Feng,[a] Mahmoud Elsabahy[b] and Hui Gao *[a]

Received 4th May 2025,
Accepted 2nd July 2025

DOI: 10.1039/d5tb01059d

rsc.li/materials-b

$H_2O_2$ plays a significant role in tumor development. However, tumor cells possess certain protective mechanisms that reduce the cytotoxic effects of $H_2O_2$. Researchers have observed a notable increase in the expression of hyaluronic acid (HA), which possesses antioxidant properties, within the tumor microenvironment. This investigation revealed that HA can mitigate oxidative damage to tumors. In response to exogenous $H_2O_2$, tumor cells enhance their production of HA as a mechanism to counteract external oxidative stress. The suppression of HA levels through hyaluronidase or ribavirin significantly heightened the cytotoxic effects of $H_2O_2$ and led to an accumulation of intracellular reactive oxygen species (ROS), ultimately inhibiting tumor cell proliferation. A formulation known as $H_2O_2$@Lip + Rib@Lip was developed, utilizing liposomes encapsulated with $H_2O_2$ and ribavirin, and was tested in murine models. The results indicated a significant reduction in tumor volume in the $H_2O_2$@Lip + Rib@Lip treatment group compared to the $H_2O_2$@Lip and Rib@Lip groups. Furthermore, these findings were accompanied by decreased levels of HA and CD44 receptors, increased levels of $H_2O_2$, and enhanced apoptosis within the tumor tissues. Therefore, in the context of ROS and related therapies, HA should be prioritized as it serves as the primary and rapid antioxidant barrier in cells. Blocking HA metabolism presents a potential strategy for enhancing oxidative stress therapy.



## 1. Introduction

The infiltration of organisms by malignant tumors remains a formidable clinical challenge, for which effective therapeutic solutions are still lacking. This unmet need has driven sustained research efforts aimed at developing novel and efficacious strategies for tumor eradication.[1,2] Reactive oxygen species (ROS) play a pivotal role in the molecular mechanisms underlying tumorigenesis and metastasis. These reactive species significantly influence intracellular signal transduction pathways and the regulation of apoptosis in malignant cells.[3] One widely studied therapeutic strategy involves the deliberate elevation of ROS levels within tumor tissues to induce oxidative stress–mediated cytotoxicity.[4,5] Tumor cells have been shown to exhibit a particular sensitivity to ROS,[6] suggesting that ROS-based therapeutic approaches hold substantial potential for advancement in cancer treatment.[7]

Among the various ROS, hydrogen peroxide ($H_2O_2$) is one of the most well-characterized. Due to their high metabolic and proliferative activity, tumor cells produce considerable amounts of $H_2O_2$.[8] The intracellular accumulation of $H_2O_2$ contributes to the activation of pro-malignant signaling pathways and promotes tumor progression. However, redox homeostasis within tumor cells is delicately balanced. Studies have shown that this balance can be disrupted by introducing exogenous agents or stimulating the endogenous production of $H_2O_2$, ultimately leading to oxidative stress and subsequent tumor cell death.[9]

Despite their vulnerability to $H_2O_2$, tumor cells are not passive targets; they have evolved sophisticated defense mechanisms to resist oxidative damage. These mechanisms have become a focal point in tumor research, with numerous investigations dedicated to understanding how malignant cells evade $H_2O_2$-induced cytotoxicity and how this resistance can be overcome to enhance therapeutic efficacy. Tumor cells employ complex antioxidant defense systems—such as the glutathione (GSH) pathway—to neutralize $H_2O_2$ and maintain redox balance.[10] Nevertheless, these antioxidant responses tend to be relatively slow to activate. Furthermore, the tumor microenvironment is typically

[a] National Key Laboratory of Advanced Separation Membrane Materials & Key Laboratory of Hollow Fiber Membrane Materials and Membrane Processes (MOE) & Tianjin Key Laboratory of Hollow Fiber Membrane Materials and Processes, School of Materials Science and Engineering, Tiangong University, Tianjin 300387, P. R. China. E-mail: huigao@tiangong.edu.cn

[b] School of Biotechnology, Badr University in Cairo, Badr City, Cairo, 11829, Egypt

† Electronic supplementary information (ESI) available. See DOI: https://doi.org/10.1039/d5tb01059d

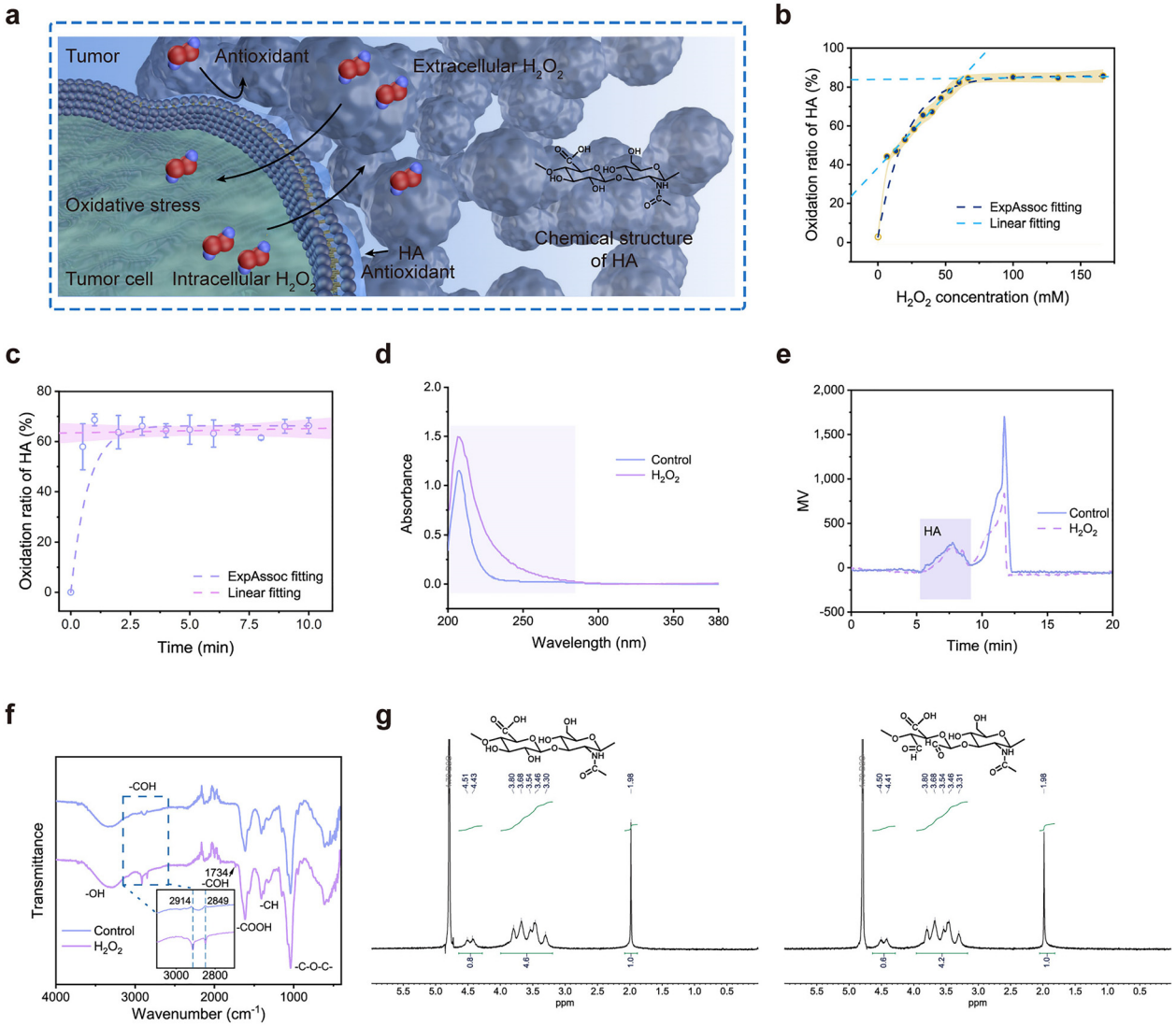


Fig. 1 *In vitro* study of $H_2O_2$ oxidation of HA. (a) The schematic diagram illustrating tumor cell resistance to both exogenous and endogenous $H_2O_2$ through the action of HA. (b) Antioxidant activity of sodium hyaluronate at different $H_2O_2$ concentrations ($n$ = 3). (c) Antioxidant activity of sodium hyaluronate against $H_2O_2$ at various time intervals ($n$ = 3). (d) UV absorption spectra of sodium hyaluronate solution. (e) GPC chromatogram of a sodium hyaluronate solution. (f) FT-IR spectra of freeze-dried sodium hyaluronate. (g) $^1$H NMR spectrum (400 MHz, $D_2O$, room temperature) of HA and after $H_2O_2$ treatment.

deficient in catalase, and catalase activity is generally lower in tumors than in normal tissues.[11] The cytotoxic effects of exogenous $H_2O_2$ are often limited by their short diffusion distance and transient half-life.[12,13] Therefore, extracellular antioxidants and cell-surface protective mechanisms often provide immediate defense against oxidative insults.

Among these extracellular components, certain polysaccharides exhibit potent antioxidant activities—most notably, hyaluronic acid (HA, Fig. 1a). HA has been documented to reduce skin aging and attenuate various forms of oxidative damage in biological systems.[14] Moreover, HA is abundantly present within the tumor microenvironment and is considered a marker of specific stages of tumor development.[15,16] The rapid upregulation of HA during tumor progression suggests a potential role in modulating redox dynamics. Notably, HA production and utilization are markedly elevated in tumors compared to normal tissues,[17,18] potentially enhancing the antioxidant capacity of tumor cells and contributing to their resistance to ROS-based therapies. However, the specific antioxidant functions of HA within the tumor microenvironment remain underexplored, and currently, no effective strategies exist to counteract its protective influence.

This study proposes the hypothesis that HA exerts significant antioxidant effects within the tumor microenvironment. To investigate this, we examined the structural alterations of HA upon exposure to $H_2O_2$. Hyaluronidase (HAse) and ribavirin[18] were utilized to enzymatically and pharmacologically deplete HA in tumors, thereby enabling a clearer assessment of tumor behavior under oxidative conditions. Furthermore, $H_2O_2$ and ribavirin were encapsulated within nanoliposomes—designated as $H_2O_2$@Lip

 

and Rib@Lip, respectively—to evaluate the antioxidative protective function of HA and its impact on therapeutic efficacy in murine tumor models. The overarching goal of this study is to offer new insights into cancer therapy, particularly in the context of oxidative stress-mediated interventions.

# 2. Experimental

## 2.1. Materials

The materials, reagents, and suppliers used in this study can be found in the ESI.†

## 2.2. *In vitro* oxidation of HA with $H_2O_2$

*In vitro* oxidation studies were carried out at 37 °C and subjected to rotational oscillation at 120 rpm. The oxidation of HA was studied with different amounts of $H_2O_2$ (0–166.7 mM) added in a 30 mL solution of 0.5% sodium hyaluronate in 0.9% normal saline (NS, pH 7.4) as the solvent. In addition, the oxidation time of $H_2O_2$ was investigated, and the incubation period was completed within 0–60 min with the addition of 33.3 mM $H_2O_2$. HA content changes were determined using the Bitter–Muir method.[19] The *in vitro* theoretical antioxidant capacity (AO) of HA was measured using the following formula (1):

$$AO = M/W \quad (1)$$

where $M$ and $W$ represent the molar mass of $H_2O_2$ and the weight of HA at a specific point with low $H_2O_2$ dosage and high oxidation ratio of HA, respectively.

## 2.3. Structure analysis of oxidized HA

0.5% HA solution with or without (control) 33.3 mM $H_2O_2$ was incubated at 37 °C and 120 rpm for 60 min under shock conditions. The UV spectrum was recorded with a LabSolutions UV-Vis spectrophotometer (Shimadzu, Japan) in the wavelength range of 200–380 nm. The molecular weight of HA was determined using an LC-20A gel permeation chromatograph (GPC; Shimadzu, Japan), with deionized water as the mobile phase. Nicolet iS5003040404 Fourier-transform infrared spectroscopy (FT-IR; Thermo Fisher Scientific, UK) was used to analyze the molecular structural changes of freeze-dried HA using a KBr pellet at wavelengths 4000–400 $cm^{-1}$, with a resolution of 4 $cm^{-1}$.

## 2.4. Cell culture

Before the cell experiments, CT26 cells were incubated for 24 h in medium without serum, in a 37 °C-environment with 5% $CO_2$ content. Among the cell culture studies, cytotoxicity, catalase activity, ELISA experiment and flow cytometry were performed using 6-well plates ($1 \times 10^6$ per well, 2.5 mL medium). The cell viability, cell proliferation activity, and ROS content were measured using 96-well plates ($1 \times 10^4$ per well, 0.1 mL medium). Except for the cell proliferation experiment, the drug tests were conducted under serum-free conditions.

## 2.5. Effect of exogenous HA, HAse, and $H_2O_2$ on tumor cells

The antioxidant effect of HA on tumor cells was evaluated by externally adding HA and HAse. 0.02–0.10% sodium hyaluronate was added to the cell well plate and incubated for 24 hours. Cell viability was evaluated using the MTT method. The DCFH-DA fluorescent probe was used to detect ROS. A FV3000 laser scanning confocal microscope (LSCM; Olympus, Japan) was utilized to observe the ROS in tumor cells. The resulting images were then analyzed using ImageJ software.

To investigate the effect of exogenous HAse on tumor cells, 0–100 U $mL^{-1}$ of HAse was added to the cell well plate and incubated for 24 hours. Tumor cell viability and ROS content were measured. After staining with calcein-AM/propidium iodide (Calcein AM/PI), cell apoptosis was measured using flow cytometry and the data was analyzed using FlowJo (10.8.1).

To investigate the effect of exogenous $H_2O_2$ on tumor cells, 0–10.0 μM $H_2O_2$ was added to the cell well plate and incubated for 24 hours. The cell viability and cytotoxicity of the tumor cells were assessed. In addition, cell vitality was evaluated simultaneously upon the addition of exogenous HAse or $H_2O_2$ and HA. The expression of HA in the tumor was determined after the administration of $H_2O_2$. The HA content of the tumor cells was measured using the ELISA method. The catalase activity of the tumor cells was assessed using a catalase kit.

## 2.6. Effect of ribavirin on tumor cells

Ribavirin was used to inhibit the expression of HA, and the HA content in the cells was verified using the ELISA method. 0–10.0 μM ribavirin was added to the cell well plate and incubated for 24 hours. ROS content, cell viability, and the cytotoxicity of the tumor cells was measured after ribavirin treatment.

## 2.7. Effect of ribavirin synergistic with $H_2O_2$ on tumor cells

To determine the enhanced effect of ribavirin on tumor cells when $H_2O_2$ is added, the concentrations of ribavirin and $H_2O_2$ were 20 μM and 2.0 μM, respectively. Cell viability, the cell cytotoxicity, catalase activity, and HA content were assessed following the administration of $H_2O_2$ and ribavirin, as described in 2.4.3. Additionally, the CD44 content on the tumor cells was evaluated using the ELISA method.

## 2.8. Assembly and characterization of nanoliposomes

Nanoliposomes were prepared according to previous reports.[20] DPPC (17.6 mg), cholesterol (6.17 mg), and DSPE-$PEG_{2000}$ (10 mg) were dissolved in dichloromethane. And then, the solvent was removed through vacuum distillation. For the fabrication of $H_2O_2$@Lip or Rib@Lip, the PBS solution containing 0.1 M $H_2O_2$ or 0.1 M ribavirin was used for hydration. The diameter of the nanoliposomes was analyzed using a Zetasizer PRO DLS (Malvern Panalytical, UK). The morphology of the nanoliposomes was analyzed using Hitachi H7650 transmission electron microscopy (TEM, HITACHI, Ltd, Japan). The nanoliposomes were placed in the dialysis setting (1000 Da), and $H_2O_2$ and ribavirin release were measured by flow

cytometer (DCFH-DA) and UV analysis (206 nm) at predetermined times, respectively.

### 2.9. Cell properties of nanoliposome treatment

The effects of $H_2O_2$@Lip and Rib@Lip on the cells were investigated. After 24 h of incubation, cellular internalization of nanoliposomes (Cy7 DiC18, DIR staining) was determined using flow cytometry. The cell viability and HA levels were measured using the MTT and ELISA methods.

### 2.10. Animals and tumor models

BALB/c male mice at 4–6 weeks old were purchased from the Beijing Vital River Laboratory Animal Technology Co., Ltd (Beijing, China). All animal studies were approved by the local ethical committee in accordance with the 'Institute Ethical Committee Guidelines' of Institute of Radiation Medicine Chinese Academy of Medical Sciences (IRM-DWLL-2022118). A CT26 tumor model was established by subcutaneous injection of CT26 cells ($1.0 \times 10^5$) suspended in 100 μL of RPMI-1640. The length ($L$) and width ($W$) of each tumor were measured with a caliper, and the tumor volume was calculated using the formula (2):

$$V = (L \times W^2)/2 \quad (2)$$

### 2.11. *In vivo* fluorescence imaging

CT26 tumor-bearing male mice were intravenously injected (i.v., 10 mg $kg^{-1}$ as nanoliposome in 100 μL PBS) with free DIR, and nanoliposome-DIR. The whole-body fluorescence images were then acquired using an IVIS Lumina XR II Imaging System at 0 (pre-injection), 2, 4, 6, 10, and 24 h post injection. Mice were sacrificed after 24 h, and the liver, kidneys, heart, lungs, spleen, and tumors were resected. Fluorescence imaging of these organs and tumors was then performed. The fluorescence intensities were quantified by measuring the region of interest (ROI) using Living Image software (LivingImage, USA).

### 2.12. Antitumor study

When the tumors reached an approximate size of 100 $mm^3$, the mice were randomly divided into four groups, with five mice in each group. The treatments were as follows (i.v., 10 mg $kg^{-1}$ based on nanoliposome, 100 μL in PBS): (1) PBS; (2) $H_2O_2$@Lip; (3) Rib@Lip; (4) $H_2O_2$@Lip + Rib@Lip was prepared using carrier nanoliposomes, and tumor characterization was assessed in the mouse model.

The HA content in the tumor tissue was quantified using ELISA. To assess the levels of $H_2O_2$ in the tumor cells, homogenized tumor tissues from treated mice were stained with DCFH-DA and analyzed *via* flow cytometry. Additionally, CD44 levels were measured using flow cytometry. The catalase activity in the tumor tissue was evaluated using a catalase assay kit. The GSH content in the tumor tissues was determined using 5, 5′-dithiobis-(2-nitrobenzoic acid) (DTNB) reagent.

### 2.13. H&E staining, AB&NFR staining and immunohistochemistry staining assay

Major organs and tumors were carefully separated and promptly fixed in 4% paraformaldehyde. The tissues were dehydrated and embedded in paraffin. Sections were sliced for hematoxylin and eosin (H&E) staining, alcian blue & nuclear fast red (AB&NFR) staining, or TdT-mediated dUTP Nick-End Labeling (TUNEL) staining. Staining images were analyzed using ImageJ software (USA, version 2.14.0).

### 2.14. Statistical analysis

All statistical analysis was performed using IBM SPSS 26. All data were represented as the mean ± SD (standard deviation) of at least three separate experiments. Statistical differences were determined using the one-way analysis of variance (ANOVA) followed by multiple comparisons ($^*P < 0.05$, $^{**}P < 0.01$, $^{***}P < 0.001$).

## 3. Results and discussion

### 3.1 *In vitro* analysis of HA oxidized by $H_2O_2$

*In vitro* experiments observed that the degradation of HA exceeded 80% when exposed to a concentration of 60 mM $H_2O_2$ in a 0.5% HA solution, as shown in Fig. 1b. However, further increases in the concentration of $H_2O_2$ did not result in a subsequent increase in the oxidation rate beyond 90%. The findings indicated that the antioxidant value of HA ranged from 120.0 μmol $mg^{-1}$ ($H_2O_2$/HA) based on theoretical calculations. Fig. 1c and Fig. S1 (ESI†) demonstrate the effect of $H_2O_2$ on the oxidation time of HA. The oxidation process was completed within 1.0 min, indicating that HA responds rapidly to $H_2O_2$. This swift oxidation of HA suggests that it may play a significant role in the tumor microenvironment. The rapid antioxidant response could have important implications for tumor cells with elevated HA metabolism. The accelerated breakdown of HA may enhance the antioxidant defense of tumor cells against ROS. During the malignant progression of tumors, a substantial amount of HA is synthesized and metabolized.[21] This suggests that HA may play a crucial role in assisting tumors in counteracting the effects of external oxidation. *In vitro* experiments demonstrated a static oxidation process, whereas the dynamic nature of HA in the tumor environment suggests that the antioxidant capacity may be enhanced within cellular surroundings.

While certain studies indicate that HA functions as an antioxidant, the existing evidence regarding these antioxidant properties is not well-defined.[22,23] In this context, this research aims to provide additional insights into the antioxidant mechanisms associated with HA. The UV absorption spectra depicted in Fig. 1d reveal that the absorption wavelength of HA remains unchanged after treatment with $H_2O_2$, which is consistent with previous findings.[24] In contrast, the UV absorption exhibited an increase of 49.6%, potentially indicating changes in the HA molecules. Meanwhile, the molecular weight of HA, measured by GPC, remains unaltered following oxidation

 

(Fig. 1e). This observation suggests that HA does not have the ability to counteract exogenous oxidation through fragmentation, which aligns with other reports.[25] The FT-IR analysis, illustrated in Fig. 1f, demonstrates the presence of dual peaks at 2914 $cm^{-1}$ and 2849 $cm^{-1}$, alongside the emergence of a distinct signal at 1734 $cm^{-1}$. This suggests that the oxidation of the *o*-hydroxyl group of glucuronic acid by $H_2O_2$ results in the generation of an aldehyde group,[26,27] as shown in Fig. 1g. Previous study indicates that the oxidation process may cause some disruption to the structure of the sugar ring.[28,29] The $^1H$ NMR spectrum reveals a reduction in the intensity of the hydroxyl peak signal, providing further evidence of alterations in the molecular configuration of HA (Fig. 1g). This study elucidates the molecular structural changes of HA affected by $H_2O_2$, providing direct evidence for the resistance of HA to $H_2O_2$.

### 3.2. HA antioxidation capacity in tumor cells.

The antioxidative protective effects of HA on tumor cells were observed in cellular experiments. The results presented in Fig. 2a demonstrate that the addition of exogenous HA did not significantly impact cell activity. Similarly, Fig. 2b shows that the addition of HA did not significantly affect the levels of ROS in the cells. Notably, following the degradation of HA by HAse, we observed a reduction in cell viability (Fig. 2c), alongside a significant increase in intracellular ROS levels (Fig. 2d, e and Fig. S2, ESI†). This finding was further corroborated by apoptosis analysis (Fig. 2f and Fig. S3, ESI†). These results indicate that cells possess the capability to utilize HA as a means of mitigating the ROS they generate.

$H_2O_2$ was recognized as a cytotoxic agent, as demonstrated by the cytotoxicity assay presented in Fig. 2g. Despite the emergence of more potent ROS in cancer therapy, the levels

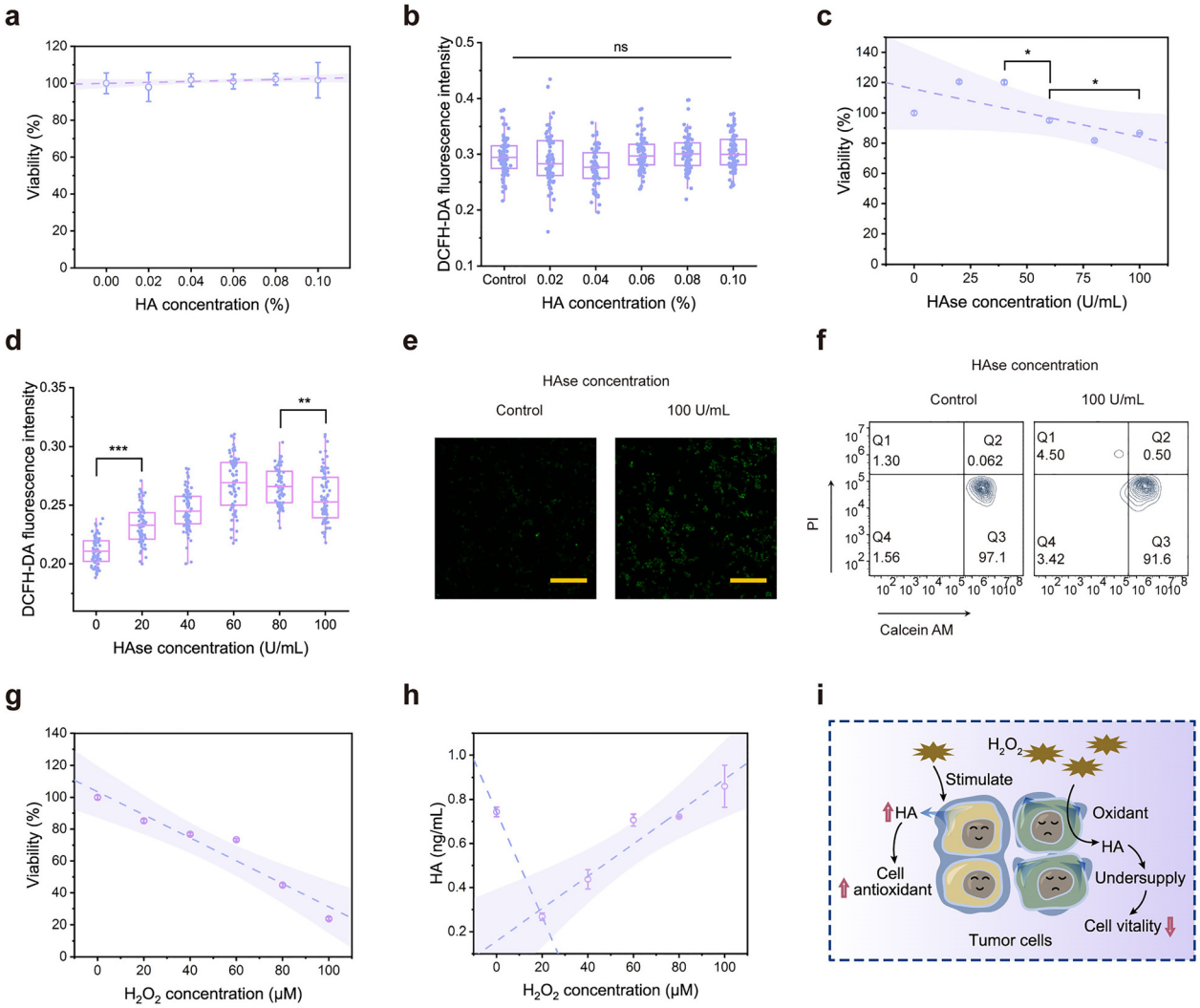


Fig. 2 Effects of exogenous HA and HAse on CT26 cells. (a) Cell viability with exogenous HA added ($n$ = 3). (b) ROS content with exogenous HA addition after DCFH-DA staining ($n$ = 3). (c) Cell viability with exogenous HAse addition. (d) ROS content with exogenous HAse addition after DCFH-DA staining. (e) LSCM images with exogenous HAse addition after DCFH-DA staining. (f) Cell cytotoxicity (calcein AM/PI) was measured by flow cytometry with the addition of exogenous HAse. (g) Cell viability with exogenous $H_2O_2$ added. (h) HA content of tumor cells with varying amounts of $H_2O_2$ added. (i) Diagram illustrating the reduction in cellular antioxidant capacity by hydrolyzing HA with HAse.

of HA in the presence of $H_2O_2$ remain insufficiently characterized. As shown in Fig. 2h, the introduction of exogenous $H_2O_2$ leads to an initial decrease in HA levels, followed by a gradual increase (Fig. 2h). This phenomenon may be attributed to the negative feedback regulation of HA in response to $H_2O_2$ stimulation. Notably, elevated concentrations of $H_2O_2$ resulted in cell mortality; however, the remaining HA levels were observed to be elevated. Furthermore, the application of exogenous $H_2O_2$ at a concentration of 40 μM did not induce an upregulation of catalase activity in the cells (Fig. S4, ESI†). Additionally, pretreatment of cells with HAse prior to $H_2O_2$ exposure enhanced the cytotoxic effects of $H_2O_2$ (Fig. S5, ESI†). Conversely, the introduction of exogenous HA prior to $H_2O_2$ treatment significantly mitigated the cytotoxicity of $H_2O_2$ (Fig. S6, ESI†), a finding that aligns with previous research.[30] These results underscore the critical role of HA as an antioxidant in tumor cells. As shown in Fig. 2i, HA can counteract the endogenous and exogenous $H_2O_2$ in tumor cells, representing an effective strategy employed by tumor cells to withstand oxidative stress. Consequently, the rapid response of HA to $H_2O_2$ suggests that HA plays a significant role as a crucial protective barrier against ROS.

### 3.3. Antioxidation of tumor cells after blocking HA by ribavirin and $H_2O_2$

The targeted degradation of HA by HAse was found to be significant. However, small molecule inhibitors are considered more suitable for drug delivery due to their enhanced stability

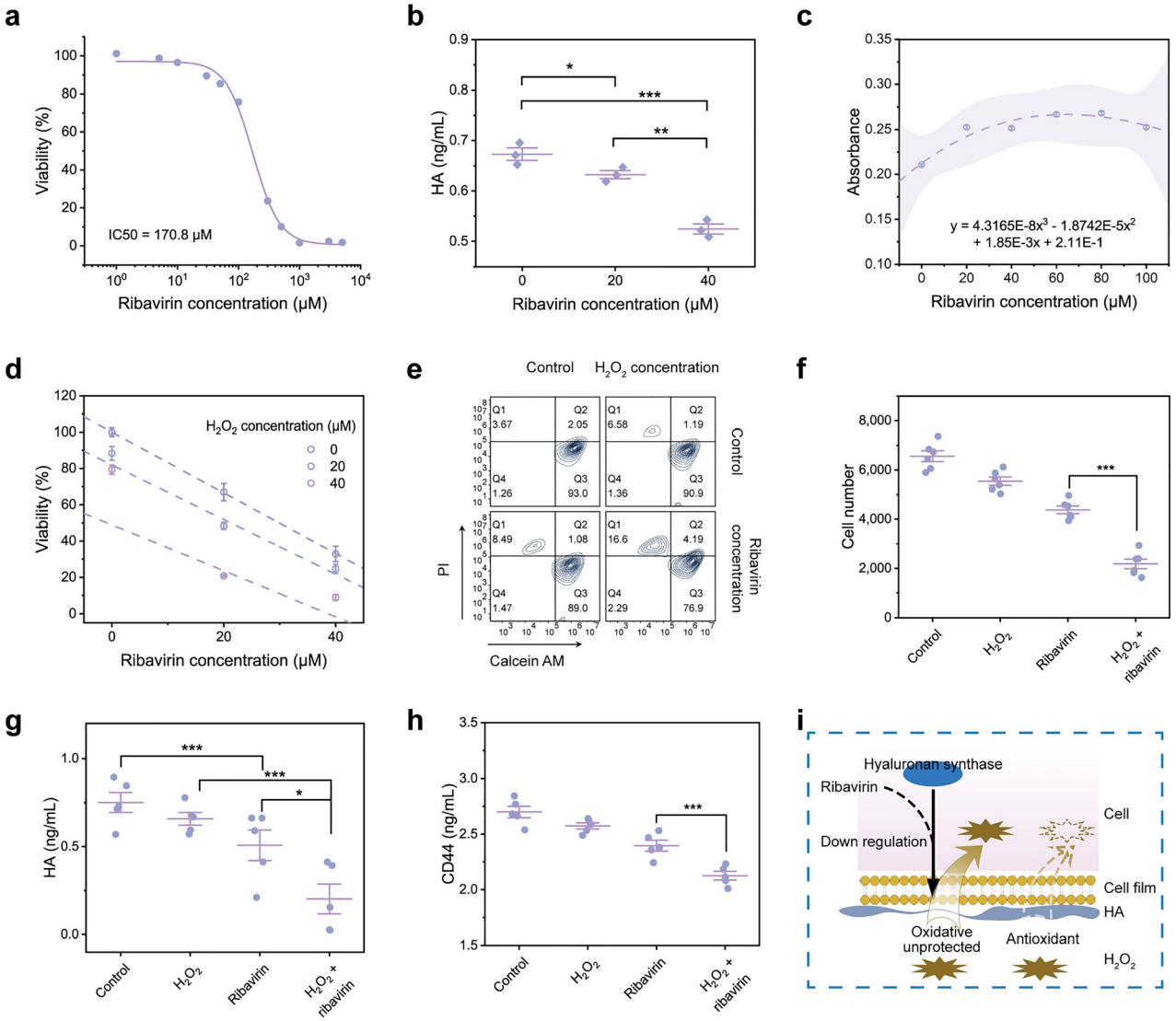


Fig. 3 Antioxidant protection of cells by HA. (a) Viabilities and IC50 of CT26 cells treated by ribavirin ($n$ = 6). (b) HA expression in tumor cells effected by ribavirin using the ELISA method. (c) The ROS content in tumor cells stained with DCFH-DA. (d) Cell viability after treatment with $H_2O_2$ (2.0 and 4.0 μM) with or without ribavirin (20 and 40 μM) to evaluate its potentiating effect ($n$ = 6). (e) Cell cytotoxicity measured by flow cytometry using Calcein AM/PI staining ($n$ = 3). (f) Cell number determined using the MTT method. (g) HA content determined using the ELISA method. (h) CD44 activity determined using the ELISA method. (i) Illustration of the synergistic effects of ribavirin and ROS on tumor cells.

and ability to penetrate biological barriers. Ribavirin has been shown to interact with eIF4E, resulting in the down-regulation of HA expression.[29,30] The administration of ribavirin produced cytotoxic effects, with an IC50 value of 170.8 μM (Fig. 3a). Furthermore, ribavirin treatment led to a notable decrease in HA level (Fig. 3b). Results from the ROS assay indicated that the reduction of HA by ribavirin was associated with an increase in ROS accumulation within the cells (Fig. 3c and Fig. S7, ESI†). Elevated concentrations of ribavirin were observed to induce cell death, accompanied by a subsequent decline in ROS levels.

The down-regulation of HA levels through the administration of ribavirin was employed to enhance the cytotoxic effects of $H_2O_2$. Cytotoxicity assessments revealed that the toxicity of $H_2O_2$ was significantly enhanced with increasing concentrations of ribavirin, demonstrating a synergistic effect ($1 + 1 > 2$), as illustrated in Fig. 3d. This phenomenon was corroborated by apoptosis assays, which indicated that ribavirin treatment resulted in a significant increase in apoptosis rates of 100.4% administered separately (Fig. 3e and Fig. S8, ESI†). Additionally, cell proliferation studies supported these findings (Fig. 3f). Notably, while $H_2O_2$ alone did not induce significant alterations in HA levels, it did enhance the inhibitory effect of ribavirin on HA levels. Specifically, cells treated with the combination of $H_2O_2$ and ribavirin exhibited a significant reduction in HA levels by 69.3% and 60.2%, respectively, compared to ribavirin treatment alone (Fig. 3g). Furthermore, the levels of the HA receptor CD44 were significantly down-regulated by 17.4% and 11.3% under these conditions (Fig. 3h). Interestingly, these treatments did not result in significant changes in catalase activity, as shown in Fig. S9 (ESI†). It is

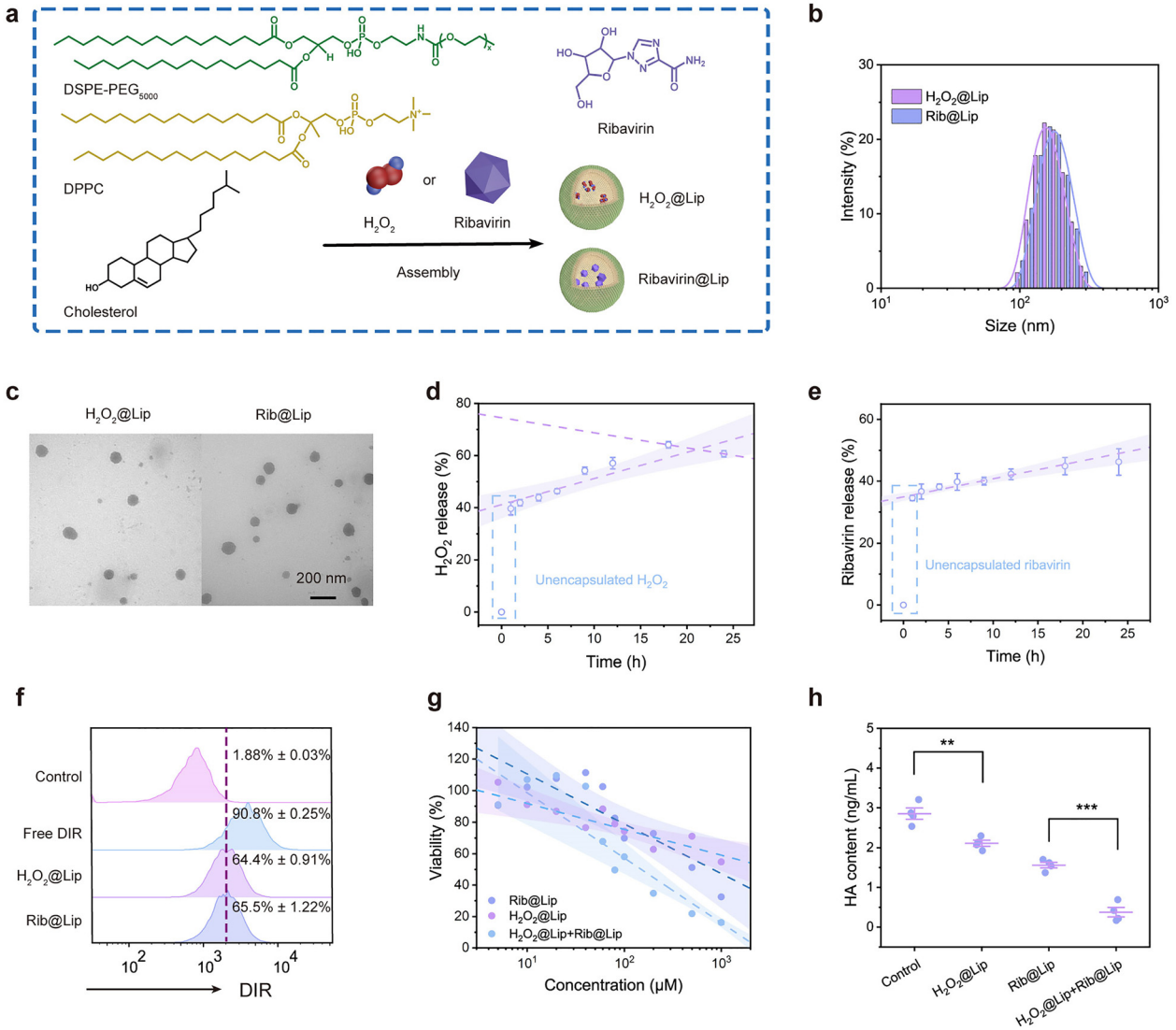


Fig. 4 Preparation, characterization, and cell experiment of $H_2O_2$@Lip and Rib@Lip. (a) Schematic illustration of nanoliposome assembly. (b) (Dynamic light scattering) DLS profiles of $H_2O_2$@Lip and Rib@Lip. (c) TEM images of $H_2O_2$@Lip and Rib@Lip. (d) $H_2O_2$ release of $H_2O_2$@Lip and Rib@Lip at 37 °C ($n$ = 3). (e) Ribavirin release of $H_2O_2$@Lip and Rib@Lip at 37 °C ($n$ = 3). (f) Cellular internalization of $H_2O_2$@Lip and Rib@Lip with DIR staining ($n$ = 3). (g) Cell viability analysis of CT26 with different nanoliposome treatment ($n$ = 6). (h) HA level analysis of CT26 cells using the ELISA method with different nanoliposome treatments ($n$ = 4).

worth noting that there are reports suggesting that $H_2O_2$ also exerts an oxidative effect on the CD44 receptor,[25] which could potentially interfere with the results of this study.

Several studies have indicated that eIF4E plays a direct role in stimulating the activity of hyaluronan synthase 3 (HAS3), which leads to the synthesis of low-molecular-weight HA and facilitates the progression of malignant tumors.[31,32] Relevant research has indicated that the synthesis of HA by HAS3 is mediated by the eIF4E pathway, with the resulting HA primarily localized on the cell surface rather than being secreted into the extracellular space.[29] It has been reported that exogenous ROS exerts an immediate and localized cytotoxic effect.[33] Meanwhile, the HA present on the cell surface can directly interact with ROS, providing a direct antioxidant effect.[34] Additionally, decreasing HA content is also associated with the rapid degradation of HA itself.[35,36] Based on the above studies, this study revealed that inhibiting HA expression and accumulating intracellular ROS are significant factors contributing to ribavirin-induced tumor cell death. Collectively, these results suggest that ribavirin can inhibit HA expression, reduce cell viability, and increase ROS accumulation, as shown in Fig. 3i. Besides, it is important to note that ribavirin-induced cytotoxicity may result in a potential amplification effect.

However, this does not negate the reduction of antioxidant protection and the synergistic enhancement of $H_2O_2$ caused by HA inhibition.

### 3.4. Characterization and cell experiment of $H_2O_2$@Lip and Rib@Lip

To further validate these concepts, a nanoliposome was prepared using DPPC, DSPE-$PEG_{2000}$, and cholesterol. $H_2O_2$ or ribavirin was encapsulated in the nanoliposome, designated as $H_2O_2$@Lip and Rib@Lip (Fig. 4a). DLS data for the nanoliposomes are presented in Fig. 4b, which also include $H_2O_2$@Lip and Rib@Lip. The morphology of the nanoliposomes was observed by TEM (Fig. 4c), revealing a spherical structure. The chemical structure of $H_2O_2$ is similar to that of water molecules, and these $H_2O_2$ encapsulated in the nanoliposomes can be released outward by passive diffusion,[20] as evidenced by the data in Fig. 4d. It is important to note that the lower stability of $H_2O_2$ necessitates the use of freshly prepared nanoliposomes for experiments. As observed from the release data of ribavirin in Fig. 4e, ribavirin is similarly released through passive diffusion. These findings contribute to the further validation of the antioxidant effect of HA *in vivo*.

The antitumor efficacy of the nanoliposomes was assessed through *in vitro* experiments. Firstly, the cellular uptake of nanoliposomes-DIR was quantified using flow cytometry. As illustrated in Fig. 4f, the cellular uptake of nanoliposomes-DIR reached 64% after incubating the nanoliposomes-DIR with CT26 cells for 6 h. Subsequently, we evaluated the cytotoxic effects of $H_2O_2$@Lip and Rib@Lip. Free drugs were removed *via* PBS dialysis over a duration of one hour. Both $H_2O_2$@Lip and Rib@Lip exhibited significant cytotoxicity towards the cells, with $H_2O_2$@Lip and Rib@Lip demonstrating enhanced cytotoxic effects, corroborating previous findings (Fig. 4g). Furthermore, $H_2O_2$@Lip + Rib@Lip resulted in a significant decrease in HA levels compared to the $H_2O_2$@Lip and Rib@Lip groups (Fig. 4h). Considering these findings, this study intends to further investigate our results using murine tumor models.

### 3.5. *In vivo* experiments of $H_2O_2$@Lip and Rib@Lip

The axillary CT26 tumor-bearing mouse model was established through subcutaneous injection. Mice were randomly assigned to receive treatment with various nanoliposomes (Fig. 5a). These nanoliposomes demonstrated the ability to penetrate tumor tissues, resulting in a reduction in HA levels within tumor cells. The nanoliposome releases ribavirin to inhibit the expression of HA and enhance the oxidative capacity of $H_2O_2$. Additionally, $H_2O_2$ can compromise the protective function of HA, disrupt its synthesis and metabolism within cells, and amplify the oxidative therapeutic effects on tumors (Fig. 5b). Notably, this study observed a significant accumulation of these nanoparticles in tumor tissues at the 6-hour mark, attributed to the enhanced permeability and retention (EPR) effect, which facilitated targeted drug release while minimizing toxicity to healthy tissues (Fig. 5c and Fig. S10, S11, ESI†). The analysis of tumor volume changes, illustrated in Fig. 5d, indicated that the administration of $H_2O_2$@Lip and Rib@Lip markedly reduced the tumor growth rate. In particular, the $H_2O_2$@Lip + Rib@Lip exhibited a more pronounced inhibitory effect on tumor growth (Fig. 5e). Histological images of tumor tissues obtained on the 10th day post-treatment are presented in Fig. 5f. Mice treated with $H_2O_2$@Lip + Rib@Lip exhibited a significant reduction in tumor volume, with a decrease of 62.2% and 55.9% in tumor weight compared to those treated with $H_2O_2$@Lip and Rib@Lip, respectively (Fig. 5g). These findings underscore the substantial therapeutic efficacy observed in the mouse model. Ribavirin was shown to inhibit HA expression, thereby enhancing the cytotoxic effects of $H_2O_2$ on tumor cells. Recent studies have indicated that $H_2O_2$ can be formulated as a more reactive free radical, and these molecules, possessing greater oxidizing potential,[37] are anticipated to yield stronger therapeutic outcomes against tumors.

### 3.6. Analysis of *in vivo* experiments

Analysis of HA content in tumor tissues revealed that exposure to $H_2O_2$ did not result in significant alterations in HA levels. In contrast, treatment with ribavirin induced a marked reduction in HA content (Fig. 6a). Notably, administration of $H_2O_2$@Lip + Rib@Lip led to a pronounced decrease in HA levels, showing a 73.7% reduction compared to the Rib@Lip group. These results indicate that exposure to $H_2O_2$ leads to a further reduction in the levels of HA when its continuous synthesis is impaired. Moreover, the decrease in HA levels was accompanied by a significant downregulation of the HA receptor CD44 (Fig. 6b and Fig. S12, ESI†), further supporting the impact of treatment on the HA-CD44 axis.

The accumulation of intracellular ROS is closely associated with the inhibition of tumor progression. As shown in Fig. 6c and Fig. S13 (ESI†), treatment with $H_2O_2$@Lip + Rib@Lip induced a substantial increase in ROS levels within tumor

 

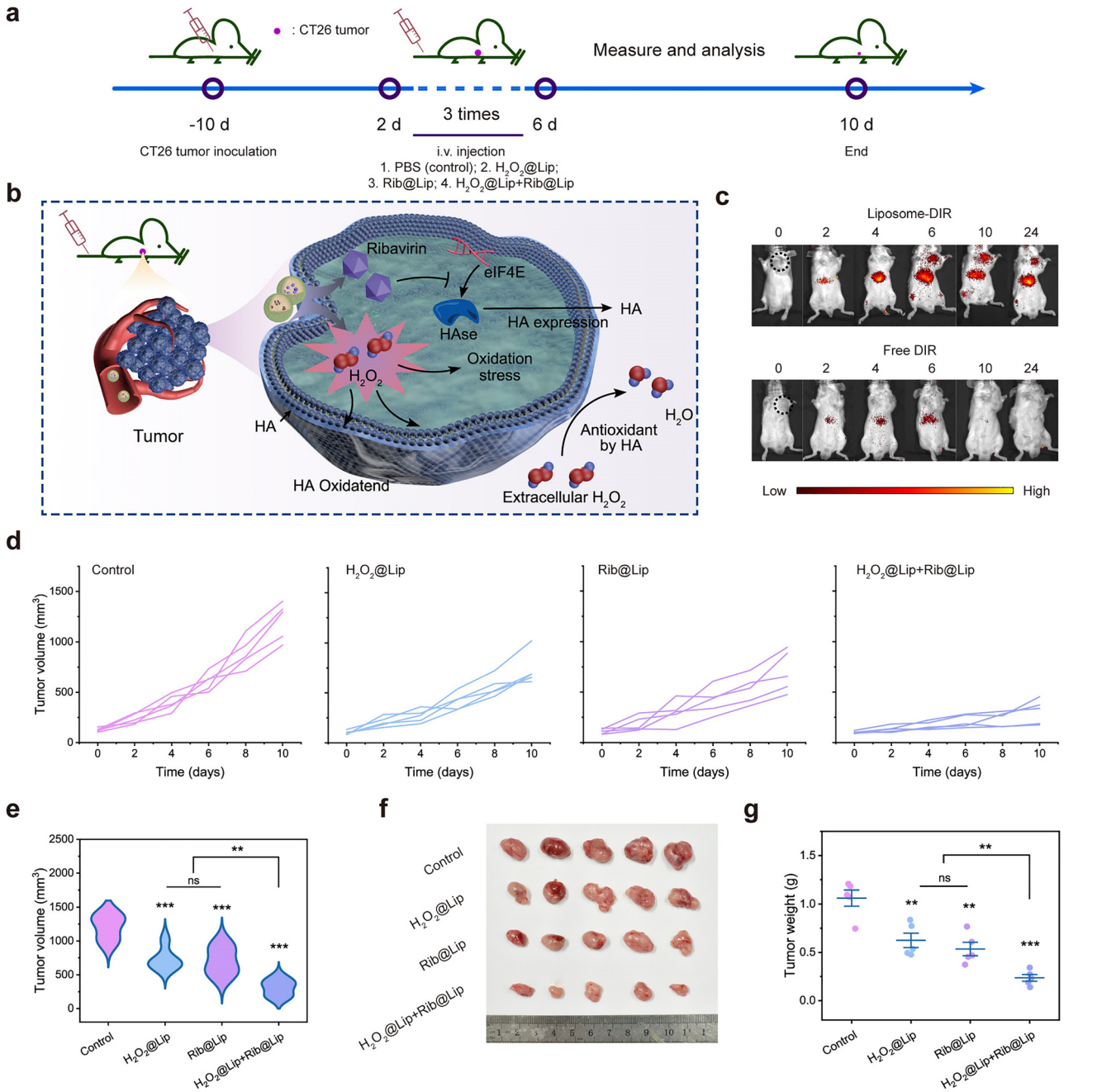


Fig. 5 *In vivo* anticancer applications of $H_2O_2$@Lip and Rib@Lip. (a) Schematic illustration of treatment schedules. CT26 cells were subcutaneously injected 10 days before treatment. From day 0, PBS (control), $H_2O_2$@Lip, Rib@Lip, or $H_2O_2$@Lip + Rib@Lip were administered every 2 days *via* i.v. injection (10 mg $kg^{-1}$). (b) Schematic of $H_2O_2$@Lip and Rib@Lip treatment and HA antioxidant protection removal for tumor therapy. (c) Representative fluorescence images of CT26 tumor-bearing mice at different timepoints after i.v. injection of free DIR or nanoliposome-DIR. (d) Tumor volume of the CT26 tumor model with $H_2O_2$@ Lip, Rib@Lip, and $H_2O_2$@Lip + Rib@Lip treatment ($n$ = 5). (e) Tumor volume analysis of different nanoliposome treatment ($n$ = 5). (f) Photo of tumor size after the treatment. (g) Tumor weight of CT26 tumor tissues with different nanoliposome treatments ($n$ = 5).

tissues, with a 282.2% increase relative to the $H_2O_2$@Lip group and a 58.0% increase compared to the Rib@Lip group, thereby promoting oxidative stress and apoptosis in tumor cells. Catalase and GSH represent key components of the tumor's antioxidant defense system.[38] However, measurements of catalase activity and GSH levels (Fig. 6d and e) revealed no significant changes across the treatment groups, highlighting the central role of HA in mediating oxidative protection under these conditions.

In this investigation, histological examination of tumor tissue *via* H&E staining revealed that the administered nanoliposomes did not exhibit toxicity toward normal tissues in murine models (Fig. S14, ESI†). Furthermore, no statistically significant differences in body weight were noted among the

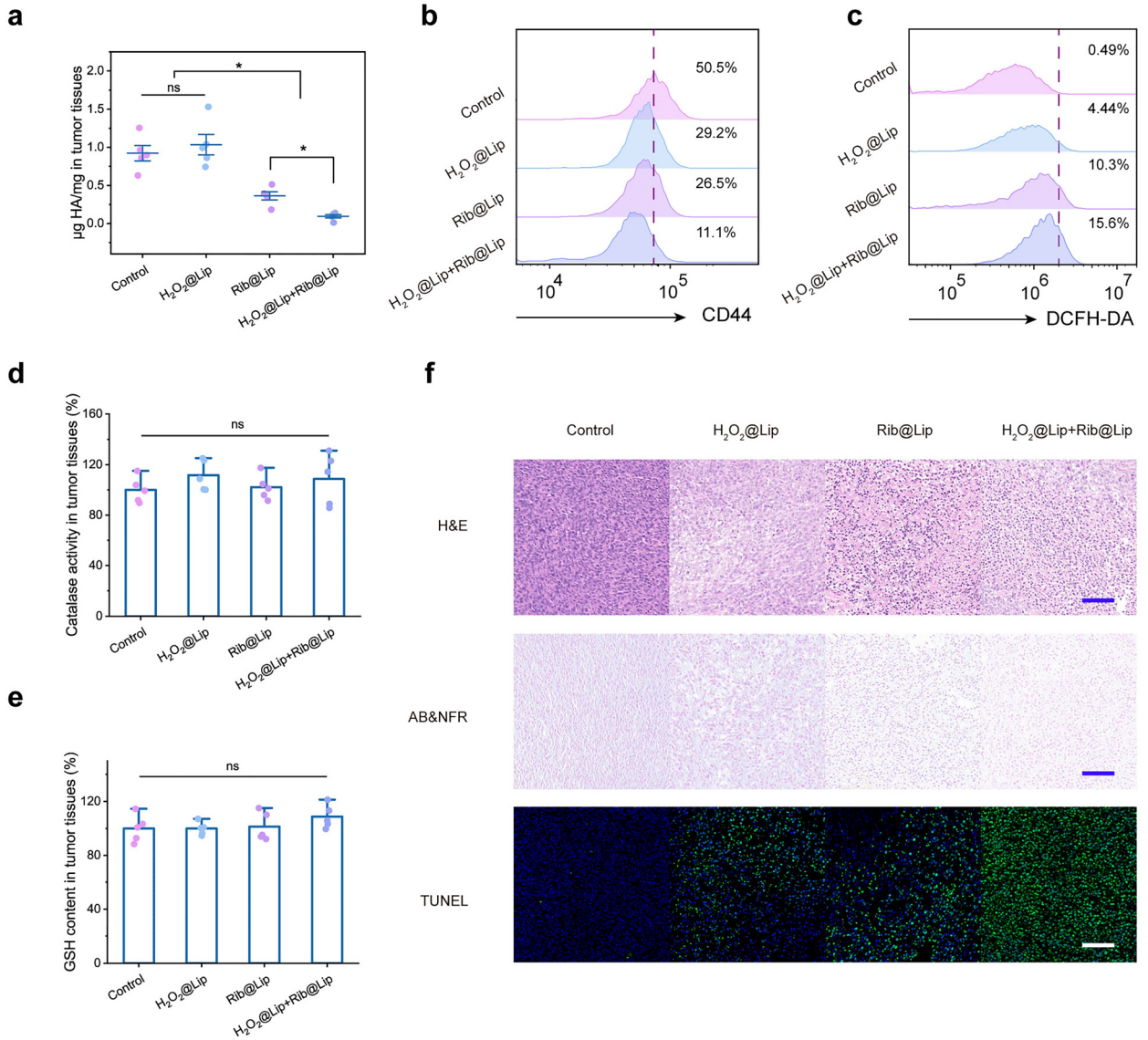


Fig. 6 Analysis of tumor tissues after different treatment. (a) HA levels measured using the ELISA method ($n$ = 5). (b) ROS content (DCFH-DA staining) in tumor tissues evaluated using a flow cytometer ($n$ = 3). (c) CD44 levels (FITC-) in tumor tissues evaluated using a flow cytometer ($n$ = 3). (d) Catalase activity analysis using catalase kit ($n$ = 5). (e) Reduced GSH in tumor tissues evaluated using the DTNB method ($n$ = 5). (f) H&E, AB&NFR, and TUNEL (blue-/green +) staining images, scale bar: 100 μm.

various treatment cohorts (Fig. S15, ESI†). Notably, nanoparticles that accumulated within the tumor tissue demonstrated an inhibitory effect on tumor cells, as evidenced by the H&E staining images (Fig. 6f). To more directly assess the levels of HA within the tumor tissue, we employed AB&NFR staining.[39] The results indicated that the blue staining area, representing HA, did not exhibit significant alterations following treatment with $H_2O_2$@Lip, whereas ribavirin treatment resulted in a marked reduction of the blue area (Fig. 6f and Fig. S16, ESI†). In the $H_2O_2$@Lip + Rib@Lip treatment group, the HA content was significantly diminished by 35.6% in comparison to the Rib@Lip group. ROS have been shown to induce cellular apoptosis,[40] a phenomenon that was corroborated by TUNEL staining (Fig. 6f and Fig. S17, ESI†). The $H_2O_2$@Lip + Rib@Lip treatment notably augmented cell apoptosis, which may serve as a critical mechanism underlying the inhibition of tumor growth. Consequently, it has been established that HA confers antioxidant protection to tumor cells, with substantial quantities of HA safeguarding these cells from oxidative damage. The application of ribavirin as an HA inhibitor may enhance oxidative tumor treatment modalities, including photodynamic therapy, chemical therapy, and other oxidative strategies, thereby yielding more favorable therapeutic outcomes.

## Conclusions

In summary, this study demonstrates that the substantial secretion of HA by tumor cells creates a direct oxidative

 

protective barrier for these cells. The application of the HA inhibitor ribavirin to reduce the levels of HA in tumor cells significantly increases the cytotoxicity of $H_2O_2$ towards these cells. Additionally, we validated the antioxidant properties of HA by employing nanoliposomes as $H_2O_2$@Lip + Rib@Lip to deliver ribavirin and $H_2O_2$ directly to the tumor tissue, where the administration of ribavirin augmented the cytotoxic effects of exogenous $H_2O_2$ on tumor cells. These findings underscore the antioxidant conferred by HA against both endogenous and exogenous ROS, which are produced in large quantities within the tumor microenvironment. Furthermore, the results emphasize that the strategic use of ribavirin to diminish tumor HA levels can enhance the efficacy of ROS-based therapeutic approaches.

## Author contributions

Hegang Lu: conceptualization, methodology, data curation, investigation, writing – original draft, formal analysis. Yunjian Yu: writing review & editing, formal analysis. Shengke Zhao: supervision, validation, investigation. Youtao Xin: methodology, investigation. Hongyu Liu: investigation. Qinghua Feng: investigation. Mahmoud Elsabahy: writing – review & editing. Hui Gao: conceptualization, resources, writing – review & editing, supervision, project administration, funding acquisition.

## Conflicts of interest

The authors declare no competing financial interest.

## Data availability

The data supporting this article have been included as part of the ESI.†

## Acknowledgements

This work was supported by the National Key R&D Program of China (2024YFE0104000), the National Natural Science Foundation of China (U20A20260 and 22075209), the Key Program of Tianjin Municipal Natural Science Foundation (No. 22JCZDJC00570), a distinguished professor of Tianjin, and the Training Project of Innovation Team of Colleges and Universities in Tianjin (TD13-5020). We would like to thank the Analytical & Testing Center of Tiangong University for TEM and $^1$H NMR testing works.

## References

1 A. Jassim, E. P. Rahrmann, B. D. Simons and R. J. Gilbertson, Cancers make their own luck: Theories of xancer origins, *Nat. Rev. Cancer*, 2023, **23**, 710–724.
2 R. L. Siegel, K. D. Miller, N. S. Wagle and A. Jemal, Cancer statistics, *Ca-Cancer J. Clin.*, 2023, **73**(1), 17–48.
3 E. C. Cheung and K. H. Vousden, The role of ROS in tumour development and progression, *Nat. Rev. Cancer*, 2022, **22**(5), 280–297.
4 K. Musaie, S. Abbaszadeh, K. Marais, V. Nosrati-Siahmazgi, S. Rezaei, B. Xiao, K. Dua, H. A. Santos and M.-A. Shahbazi, $H_2O_2$-generating advanced nanomaterials for cancer treatment, *Adv. Funct. Mater.*, 2025, DOI: 10.1002/adfm.202425866.
5 Z. Xu, R. Fan, X. Zhang, Y. Guo, S. Tan, Y. Li, Y. Yan, J. Gao, W. Xue, D. Wang and D. Gao, Regulation of ROS balance in the tumor microenvironment achieves reversal of immune suppression and deep penetration of nanomedicines, *Chem. Eng. J.*, 2025, **505**, 159716.
6 A. R. Gibson, B. R. O'Leary, J. Du, E. H. Sarsour, A. L. Kalen, B. A. Wagner, J. M. Stolwijk, K. C. Falls-Hubert, M. S. Alexander, R. S. Carroll, D. R. Spitz, G. R. Buettner, P. C. Goswami and J. J. Cullen, Dual oxidase-induced sustained generation of hydrogen peroxide contributes to pharmacologic ascorbate-induced cytotoxicity, *Cancer Res.*, 2020, **80**(7), 1401–1413.
7 D. Kalyane, D. Choudhary, S. Polaka, H. Goykar, T. Karanwad, K. Rajpoot and R. Kumar Tekade, Reactive oxygen nanogenerators for cancer therapy, *Prog. Mater. Sci.*, 2022, **130**, 100974.
8 Z. Chu, J. Yang, W. Zheng, J. Sun, W. Wang and H. Qian, Recent advances on modulation of $H_2O_2$ in tumor microenvironment for enhanced cancer therapeutic efficacy, *Coord. Chem. Rev.*, 2023, **481**, 215049.
9 H. Sies and D. P. Jones, Reactive oxygen species (ROS) as pleiotropic physiological signalling agents, *Nat. Rev. Mol. Cell Biol.*, 2020, **21**(7), 363–383.
10 X. An, W. Yu, J. Liu, D. Tang, L. Yang and X. Chen, Oxidative cell death in cancer: mechanisms and therapeutic opportunities, *Cell Death Dis.*, 2024, **15**, 556.
11 S. Abdalbagemohammedabdalsadeg, B.-L. Xiao, X.-X. Ma, Y.-Y. Li, J.-S. Wei, A. A. Moosavi-Movahedi, R. Yousefi and J. Hongs, Catalase immobilization: Current knowledge, key insights, applications, and future prospects - A review, *Int. J. Biol. Macromol.*, 2024, **276**, 133941.
12 C. Jia, Y. Guo and F. Wu, Chemodynamic Therapy via Fenton and Fenton-like nanomaterials: Strategies and recent advances, *Small*, 2022, **18**(6), 2103868.
13 J. Qi, G. Jiang, Y. Wan, J. Liu and F. Pi, Nanomaterials-modulated Fenton reactions: Strategies, chemodynamic therapy and future trends, *Chem. Eng. J.*, 2023, **466**, 142960.
14 S. Hussain, Z. Ji, A. J. Taylor, L. M. DeGraff, M. George, C. J. Tucker, C. H. Chang, R. Li, J. C. Bonner and S. Garantziotis, Multiwalled carbon nanotube functionalization with high molecular weight hyaluronan significantly reduces pulmonary injury, *ACS Nano*, 2016, **10**(8), 7675–7688.
15 A. M. Carvalho, R. L. Reis and I. Pashkuleva, Hyaluronan receptors as mediators and modulators of the tumor microenvironment, *Adv. Healthcare Mater.*, 2023, **12**(5), 2202118.
16 S. S. Skandalis, T. Karalis and P. Heldin, Intracellular hyaluronan: Importance for cellular functions, *Semin. Cancer Biol.*, 2020, **62**, 20–30.
17 Z. Liu, P. Hou, J. Fang, C. Shao, Y. Shi, G. Melino and A. Peschiaroli, Hyaluronic acid metabolism and chemotherapy

resistance: Recent advances and therapeutic potential, *Mol. Oncol.*, 2024, **18**(9), 2087–2106.
18 F. Volpin, J. Casaos, J. Sesen, A. Mangraviti, J. Choi, N. Gorelick, J. Frikeche, T. Lott, R. Felder, S. J. Scotland, T. S. K. Eisinger-Mathason, H. Brem, B. Tyler and N. Skuli, Use of an anti-viral drug, ribavirin, as an anti-glioblastoma therapeutic, *Oncogene*, 2017, **36**(21), 3037–3047.
19 T. Bitter and H. M. Muir, A modified uronic acid carbazole reaction, *Anal. Biochem.*, 1962, **4**(4), 330–334.
20 X. Song, J. Xu, C. Liang, Y. Chao, Q. Jin, C. Wang, M. Chen and Z. Liu, Self-supplied tumor oxygenation through separated liposomal delivery of $H_2O_2$ and catalase for enhanced radioimmunotherapy of cancer, *Nano Lett.*, 2018, **18**(10), 6360–6368.
21 T. Chanmee, P. Ontong and N. Itano, Hyaluronan: A modulator of the tumor microenvironment, *Cancer Lett.*, 2016, **375**(1), 20–30.
22 N. T.-P. Nguyen, L. V.-H. Nguyen, N. M.-P. Tran, D. T. Nguyen, T. N.-T. Nguyen, H. A. Tran, N. N.-T. Dang, T. V. Vo and T.-H. Nguyen, The effect of oxidation degree and volume ratio of components on properties and applications of in situ cross-linking hydrogels based on chitosan and hyaluronic acid, *Mater. Sci. Eng., C*, 2019, **103**, 109670.
23 N. Chen, T. Jiang, J. Xu, W. Xi, E. Shang, P. Xiao and J. Duan, The relationship between polysaccharide structure and its antioxidant activity needs to be systematically elucidated, *Int. J. Biol. Macromol.*, 2024, **270**, 132391.
24 H. Chen, J. Qin and Y. Hu, Efficient degradation of high-molecular-weight hyaluronic acid by a combination of ultrasound, hydrogen peroxide, and copper ion, *Molecules*, 2019, **24**(3), 617.
25 M. Yusupov, A. Privat-Maldonado, R. M. Cordeiro, H. Verswyvel, P. Shaw, J. Razzokov, E. Smits and A. Bogaerts, Oxidative damage to hyaluronan-CD44 interactions as an underlying mechanism of action of oxidative stress-inducing cancer therapy, *Redox Biol.*, 2021, **43**, 101968.
26 D. J. Gorelik, V. Dimakos, T. Adrianov and M. S. Taylor, Photocatalytic, site-selective oxidations of carbohydrates, *Chem. Commun.*, 2021, **57**(91), 12135–12138.
27 D. Li, M. Tohti, Y. Fu, Y. Zhang, Z. Xiong, J. Li and Y.-F. Guo, Aldehyde group pendant-grafted pectin-based injectable hydrogel, *Int. J. Biol. Macromol.*, 2024, **264**, 130453.
28 O. Smidsrød and T. Painter, Effect of periodate oxidation upon the stiffness of the alginate molecule in solution, *Carbohydr. Res.*, 1973, **26**(1), 125–132.
29 W. Mubarok, K. C. M. L. Elvitigala, M. Nakahata, M. Kojima and S. Sakai, Modulation of cell-cycle progression by hydrogen peroxide-mediated cross-linking and degradation of cell-adhesive hydrogels, *Cells*, 2022, **11**(5), 881.
30 J. Shi, Y. Wang, L. Zhang, F. Wang, Y. Miao, J. Yang, L. Wang, S. Shi, L. Ma and J. Duan, Inorganic catalase-powered nanomotors with hyaluronic acid coating for pneumonia therapy, *Int. J. Biol. Macromol.*, 2024, **270**, 132028.
31 H. A. Zahreddine, B. Culjkovic-Kraljacic, A. Emond, F. Pettersson, R. Midura, M. Lauer, S. Del Rincon, V. Cali, S. Assouline, W. H. Miller, V. Hascall and K. L. Borden, The eukaryotic translation initiation factor eIF4E harnesses hyaluronan production to drive its malignant activity, *eLife*, 2017, **6**, e29830.
32 S. Assouline, B. Culjkovic-Kraljacic, J. Bergeron, S. Caplan, E. Cocolakis, C. Lambert, C. J. Lau, H. A. Zahreddine, W. H. Miller and K. L. B. Borden, A phase I trial of ribavirin and low-dose cytarabine for the treatment of relapsed and refractory acute myeloid leukemia with elevated eIF4E, *Haematologica*, 2015, **100**(1), e7–e9.
33 S. Assouline, B. Culjkovic, E. Cocolakis, C. Rousseau, N. Beslu, A. Amri, S. Caplan, B. Leber, D.-C. Roy, W. H. Miller and K. L. B. Borden, Molecular targeting of the oncogene eIF4E in acute myeloid leukemia (AML): A proof-of-principle clinical trial with ribavirin, *Blood*, 2009, **114**(2), 257–260.
34 L. Volpon, B. Culjkovic-Kraljacic, M. J. Osborne, A. Ramteke, Q. Sun, A. Niesman, Y. M. Chook and K. L. B. Borden, Importin 8 mediates $m^7G$ cap-sensitive nuclear import of the eukaryotic translation initiation factor eIF4E, *Proc. Natl. Acad. Sci. U. S. A.*, 2016, **113**(19), 5263–5268.
35 X. Zhang, X. Zhang, H. Guo, S. Jia, Y. Li, S. Xing, J. Chang and S. Wang, A photo-activated continuous reactive oxygen species nanoamplifier for dual-dynamic cascade cancer therapy, *Adv. Healthcare Mater.*, 2023, **12**(28), 2301469.
36 S. Garantziotis, Modulation of hyaluronan signaling as a therapeutic target in human disease, *Pharmacol. Ther.*, 2022, **232**, 107993.
37 C. Glorieux, S. Liu, D. Trachootham and P. Huang, Targeting ROS in cancer: Rationale and strategies, *Nat. Rev. Drug Discovery*, 2024, **23**(8), 583–606.
38 B. Halliwell, Understanding mechanisms of antioxidant action in health and disease, *Nat. Rev. Mol. Cell Biol.*, 2024, **25**(1), 13–33.
39 G. Li, Y. Fan, L. Lin, R. Wu, M. Shen and X. Shi, Two-dimensional LDH nanodisks modified with hyaluronidase enable enhanced tumor penetration and augmented chemotherapy, *Sci. China: Chem.*, 2021, **64**(5), 817–826.
40 S. Li, J. E, X. Zhao, R. Xie, J. Wu, L. Feng, H. Ding, F. He and P. Yang, Hetero-trimetallic atom catalysts enable targeted ROS generation and redox signaling for intensive apoptosis and ferroptosis, *Adv. Mater.*, 2025, **37**(19), 2417198.

 